Escherichia coli alkaline phosphatase: X-ray structural studies of a mutant enzyme (His-412 → Asn) at one of the catalytically important zinc binding sites

ARTICLE *in* PROTEIN SCIENCE · AUGUST 1995

Impact Factor: 2.85 · DOI: 10.1002/pro.5560040807 · Source: PubMed

3 AUTHORS, INCLUDING:

Thomas T Tibbitts
Infinity Pharmaceuticals
11 PUBLICATIONS **357** CITATIONS

Protein Science (1995), *4*:1498–1506. Cambridge University Press. Printed in the USA.

Escherichia coli alkaline phosphatase: X-ray structural studies of a mutant enzyme (His-412 → Asn) at one of the catalytically important zinc binding sites

LAN MA, THOMAS T. TIBBITTS, AND EVAN R. KANTROWITZ

Department of Chemistry, Merkert Chemistry Center, Boston College, Chestnut Hill, Massachusetts 02167

(RECEIVED April 11, 1995; ACCEPTED June 6, 1995)

Abstract

The X-ray structure of a mutant version of *Escherichia coli* alkaline phosphatase (H412N) in which His-412 was replaced by Asn has been determined at both low (−Zn) and high (+Zn) concentrations of zinc. In the wild-type structure, His-412 is a direct ligand to one of the two catalytically critical zinc atoms (Zn_1) in the active site. Characterization of the H412N enzyme in solution revealed that the mutant enzyme required high concentrations of zinc for maximal activity and for high substrate and phosphate affinity (Ma L, Kantrowitz ER, 1994, *J Biol Chem 269*:31614–31619). The H412N enzyme was also inhibited by Tris, in contrast to the wild-type enzyme, which is activated more than twofold by 1 M Tris. To understand these kinetic properties at the molecular level, the structure of the H412N(+Zn) enzyme was refined to an *R*-factor of 0.174 at 2.2 Å resolution, and the structure of the H412N(−Zn) enzyme was refined to an *R*-factor of 0.166 at a resolution of 2.6 Å. Both indicated that the Asn residue substituted for His-412 did not coordinate well to Zn_1. In the H412N(−Zn) structure, the Zn_1 site had very low occupancy and the phosphate was shifted by 1.8 Å from its position in the wild-type structure. The Mg binding site was also affected by the substitution of Asn for His-412. Both structures of the H412N enzyme also revealed a surface-accessible cavity near the Zn_1 site that may serve as a binding site for Tris. The binding of Tris at the Zn_1 site may block Zn^{2+} binding at this site, which would account for the reduced affinity of the H412N enzyme for substrate as well as its reduced catalytic efficiency in the presence of Tris. Thus, the replacement of His-412 with Asn affects all three metal binding sites, suggesting that the relative positions of the metals bound at the active site of *E. coli* alkaline phosphatase are strongly linked and critical for efficient catalysis.

Keywords: metal binding site; metalloenzymes; protein structure–function; site-specific mutagenesis; X-ray diffraction

Alkaline phosphatase (EC 3.1.3.1) is a nonspecific phosphomonoesterase found in most organisms (Coleman, 1992) that catalyzes the hydrolysis reaction via a phosphoseryl intermediate (Schwartz & Lipmann, 1961; Engström, 1962) to produce inorganic phosphate and the corresponding alcohol. The enzyme will also transfer the phosphate to a hydroxyl group of an acceptor, such as ethanolamine or Tris (Dayan & Wilson, 1964; Wilson et al., 1964). The dimeric metalloenzyme from *Escherichia coli* has been extensively studied (for a review see Coleman, 1992) and its X-ray structure solved and eventually refined to 2.0 Å resolution (Sowadski et al., 1983, 1985; Kim & Wyckoff, 1991).

In the X-ray structure, the active site of each monomer contains two zinc ions and one magnesium ion (Fig. 1; Kinemage 1) in a pocket created by the termination of a number of helices and sheets that is open to the surface (Kim & Wyckoff, 1991). Inorganic phosphate is held firmly in the active site by the two zinc atoms (Zn_1[1] and Zn_2) and Arg-166. Zn_1 and Zn_2 are 4.0 Å apart and are well positioned to participate in stabilization of the trigonal bipyramidal transition state. The amino acid residues that serve as ligands to Zn_1 are His-331, His-412, and

Reprint requests to: Evan R. Kantrowitz, Department of Chemistry, Merkert Chemistry Center, Boston College, Chestnut Hill, Massachusetts 02167; e-mail: kantrowitz@hermes.bc.edu.

Abbreviations: H412N, the mutant alkaline phosphatase that has His-412 replaced by Asn; H412N(−Zn), the structure of the H412N enzyme determined with crystals that did not have added zinc in the stabilization buffer; H412N(+Zn), the structure of the H412N enzyme determined with crystals soaked in stabilization buffer containing 10 mM zinc chloride; P_i, inorganic phosphate; RMSD, RMS displacement; Zn_1, Zn_2, and Mg sites correspond to the M1, M2, and M3 sites as identified in the X-ray structure of the wild-type enzyme (Sowadski et al., 1983); Zn_1, the Zn^{2+} ion bound in the M1 site of alkaline phosphatase; Zn_2, the Zn^{2+} ion bound in the M2 site of alkaline phosphatase; Mg, the Mg^{2+} ion bound in the M3 site of alkaline phosphatase.

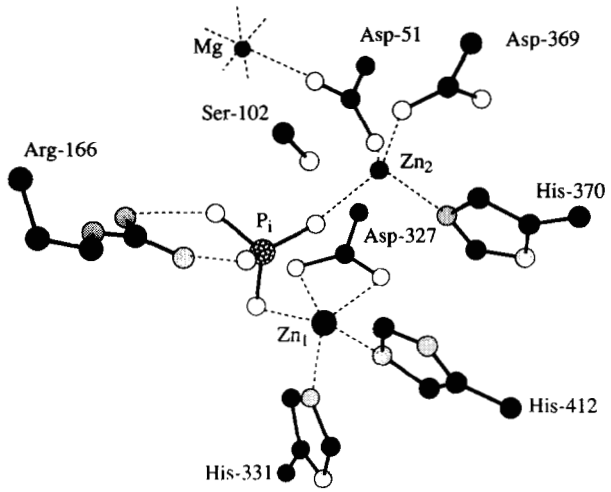

Fig. 1. Active site of *E. coli* alkaline phosphatase. Shown are Zn_1, Zn_2, Mg, phosphate (P_i), and side-chain ligands. The side chain of Asp-51, which bridges the Mg and Zn_2 sites, is also shown here; for clarity, the other ligands to Mg are not shown. Zn_1 interacts with an imidazole nitrogen of His-412 and His-331, one of the phosphate oxygens, and the carboxylate oxygens of Asp-327. Zn_2 is coordinated to Asp-369, His-370, phosphate, and Asp-51. Also shown is Ser-102, which is phosphorylated during the reaction, and Arg-166, which interacts with the phosphate.

Asp-327, whereas the amino acid residues that are ligands to Zn_2 are His-370, Asp-51, and Asp-369 (Fig. 1; Kinemage 2). The Mg site, which is 5 Å from the Zn_2 site and 7 Å from the Zn_1 site, may be occupied by either magnesium or by zinc in the absence of magnesium (Simpson & Vallee, 1968; Anderson et al., 1975; Kim & Wyckoff, 1991).

Based on biochemical and X-ray structural studies, a double in-line nucleophilic displacement mechanism has been proposed for the *E. coli* enzyme (Kim & Wyckoff, 1991; Coleman, 1992), which involves attack at the phosphorus by the hydroxyl group of Ser-102 in the first step and by a water molecule coordinated to Zn_1 in the second step. In the first half of the reaction, Zn_2 interacts with the hydroxyl of Ser-102 to stabilize the deprotonated form of the serine necessary for nucleophilic attack on the phosphorus and Zn_1 stabilizes the negative charge on the leaving group. In the second half of the reaction, Zn_2 stabilizes the negative charge on the serine hydroxyl and Zn_1 lowers the pK_a of a coordinated water molecule sufficiently for it to act as a nucleophile. In transphosphorylation, the Zn_1 activates an alcohol acceptor instead of a water molecule.

Work in this laboratory has focused on determining the role of the metals in *E. coli* alkaline phosphatase by a combination of site-specific mutagenesis and X-ray crystallography. For example, replacement of Asp-153 by His resulted in an enzyme with an altered pH profile and enhanced activity in the presence of excess Mg^{2+} (Janeway et al., 1993). The X-ray structure of this enzyme, without excess Mg^{2+}, indicated that the enzyme exists with Zn^{2+} in the Mg site (Murphy et al., 1993). These results suggested an explanation for the Mg activation of some mammalian alkaline phosphatases (Cathala et al., 1975). In these mammalian alkaline phosphatases, the enzyme as isolated may have Zn^{2+} in the Mg site. In another study, Asp-369, a ligand to Zn_2, was replaced by Ala and Asn (Tibbitts et al., 1994). The X-ray structure of the D369N enzyme revealed that only the Zn_1 site was occupied, and furthermore, the data suggested an alternative mechanism for this enzyme involving only one metal (Zn_1) with the possible assistance of His-370 (Tibbitts et al., 1994).

In order to evaluate the role of Zn_1 in *E. coli* alkaline phosphatase and the specificity of the His–Zn_1 interaction, site-specific mutagenesis was used to replace His-412 with Asn (Ma & Kantrowitz, 1994). The H412N enzyme exhibited reduced activity, lower catalytic efficiency, and weaker affinity for zinc and phosphate compared to the wild-type enzyme (Ma & Kantrowitz, 1994, and Table 1). The kinetic parameters of the H412N enzyme exhibited a strong zinc dependence (see Table 1). In the presence of optimal amounts of added zinc (0.2 mM), the k_{cat}/K_m ratio increased about 60-fold compared to the ratio in the absence of zinc. In fact, the k_{cat}/K_m ratio is nearly 1/2 of the value for the wild-type enzyme under optimal concentrations of zinc. Furthermore, Tris inhibited the H412N enzyme, which could be reversed by addition of Zn^{2+}. In order to understand these kinetic results at the molecular level, and to investigate further the role of metals in catalysis, the X-ray structure of the H412N alkaline phosphatase was determined both at low and high concentrations of zinc.

Results

Structure of H412N alkaline phosphatase in the presence of zinc

The H412N enzyme crystallized in the same space group and with unit cell dimensions similar to the crystals of the wild-type enzyme (see Table 2). The structure obtained with crystals soaked in stabilization buffer containing 10 mM zinc chloride

Table 1. *Summary of kinetic parameters for the wild-type and H412N enzymes at pH 8.0*[a]

Enzyme[b]	$[Zn^{2+}]$ (mM)	k_{cat}[c] (s^{-1})	K_m (μM)	$k_{cat}/K_m \times 10^{-6}$ ($M^{-1}\ s^{-1}$)
A) In the absence of the phosphate acceptor[d]				
Wild-type	0	31 (±1)	7 (±2)	4.4
Wild-type	0.2	32 (±2)	7 (±1)	4.6
H412N	0	7 (±0.5)	210 (±5)	0.033
H412N	0.2	18 (±0.8)	9 (±1)	2.0
B) In the presence of the phosphate acceptor[e]				
Wild-type	0	86 (± 6)	22 (±2)	3.9
Wild-type	0.2	86 (±9)	21 (±3)	4.1
H412N	0	<0.002	380 (±50)	$<5.2 \times 10^{-6}$
H412N	0.2	80 (±5)	230 (±10)	0.35

[a] Kinetic data were determined at 25 °C with *p*-nitrophenyl phosphate as substrate at pH 8.0 (Ma & Kantrowitz, 1994).

[b] Both the H412N and the wild-type enzyme were dialyzed versus 0.01 M Tris, 10^{-3} M $MgCl_2$, 10^{-4} M NaH_2PO_4, 0.31×10^{-2} M NaN_3, pH 7.4 buffer before use.

[c] The k_{cat} values are calculated from the V_{max} by use of a dimer molecular weight of 94,000. The k_{cat} per active site would be half of the value indicated.

[d] 0.01 M Tris was used as reaction buffer adjusted to pH 8.0 with HCl and the ionic strength to 0.5 with NaCl.

[e] 1.0 M Tris was used as reaction buffer; the pH was adjusted to 8.0 with HCl.

Table 2. *Summary of data collection for H412N alkaline phosphatase*

Enzyme form	Space group	d_{min} (Å)	$\frac{1}{s}$[a]	Reflections (total unique)	Completeness	Redundancy	Unit cell (Å)	Overall R_{merge}[b]
H412N(−Zn)	I222	2.6	1.6	177,067 38,252	98%	4.6	$a = 194.8$ $b = 167.7$ $c = 76.2$	0.108
H412N(+Zn)	I222	2.2	1.7	224,987 63,998	99%	3.5	$a = 194.9$ $b = 167.4$ $c = 76.5$	0.087

[a] Reciprocal of the signal-to-noise ratio in the highest resolution shell.

[b] $R_{merge} = \dfrac{\sum_{hkl}\sum_{i}|I_{mean} - I_i|}{\sum_{hkl}\sum_{i} I_i}$.

(H412N[+Zn]) was refined using X-PLOR (Brünger, 1992) to an R-factor of 0.174 at a resolution of 2.2 Å with reasonable stereochemistry (Table 3). As seen in Figure 2A, the overall structure of the H412N(+Zn) enzyme was very similar to that of the wild-type enzyme (Kim & Wyckoff, 1991). The average RMSDs between the H412N(+Zn) and wild-type structures were 0.18 Å for the α-carbon and 0.47 Å for the side-chain positions. A Luzzati plot of the resolution dependence of the crystallographic R-factor (Fig. 3) indicated that the uncertainty in the coordinates of this structure was approximately ±0.25 Å (Luzzati, 1952).

Of a total of 892 residues in the two subunits, 99.7% were within the most favored or additional allowed regions in a Ramachandran plot of the dihedral angles (Fig. 4). Two regions of the molecule had very weak electron density: the first three residues and the loop formed by residues 407–411, inclusive. The three residues at the N-terminus were not included in the refinement. The 407–411 loop was previously observed to have weak electron density in the structures of the wild-type, the D153H, and the D369H enzymes (Kim & Wyckoff, 1991; Murphy et al., 1993; Tibbitts et al., 1994) and probably represents a flexible portion of the molecule. Due to this lack of electron density, the refined coordinates of these residues have a much larger uncertainty than the overall structure.

The major differences between the H412N(+Zn) and the wild-type structures were detected in the active-site region of the mutant enzyme. During the initial refinement, full occupancy of the Zn_1 site was assumed. Inspection of the electron density maps ($2F_o - F_c$) as well as the temperature factors suggested that the Zn_1 site was only partially occupied (Fig. 5). Refinement indicated that this site was only about 20% occupied. The refined position of Zn_1 was about 1.3 Å away from its position in the wild-type structure (Kim & Wyckoff, 1991). The density for His-331, which is a ligand to Zn_1 in the wild-type structure (Kim & Wyckoff, 1991), was weak. This supports the observation that the Zn_1 site was not fully occupied in the H412N(+Zn) structure. However, the coordination between Zn_1 and its ligands His-331, Asp-327, and phosphate could still be distinguished (Fig. 5). The side chain of Asn-412 was in a position similar to that of the side chain of His-412 in the structure of the wild-type enzyme; however, the shorter side chain of Asn-412 reduced its ability to coordinate to Zn_1.

The phosphate bound 1.7 Å away from its position in the wild-type structure shifted toward the partially occupied Zn_1 site (Fig. 6). In the H412N(+Zn) structure, the binding of phosphate was mediated by the two guanidinium nitrogens of Arg-166, by a hydrogen bond to the amide of Asn-412, and by coordination to Zn_1. The phosphate actually bound away from the inside of the binding pocket and no longer interacted with Zn_2. The phosphate in the active site had a temperature factor of 30 Å^2, significantly higher than the 19-Å^2 value observed in the structure of the wild-type enzyme (Kim & Wyckoff, 1991).

In the H412N(+Zn) structure, the Zn_2 site was 90% occupied, and the positions of the side chains around the Zn_2 site was almost identical to the Zn_2 site in the wild-type structure, except that the phosphate was no longer coordinated to Zn_2. The function of Zn_2 is to activate the hydroxyl of Ser-102 for nucleophilic displacement. The side chain of Ser-102 was shifted

Table 3. *Refinement statistics for the H412N alkaline phosphatase structures*

Enzyme form	Final R-factor	d_{min} (Å)	Metals and phosphate present	Waters	RMS deviations		
					Bond lengths (Å)	Bond angles	Improper dihedral angles
H412N(−Zn)	0.166	2.6	Zn_2, Mg, P_i	219	0.02	2.01°	1.67°
H412N(+Zn)	0.174	2.2	Zn_1, Zn_2, Mg, P_i	239	0.02	2.03°	1.58°

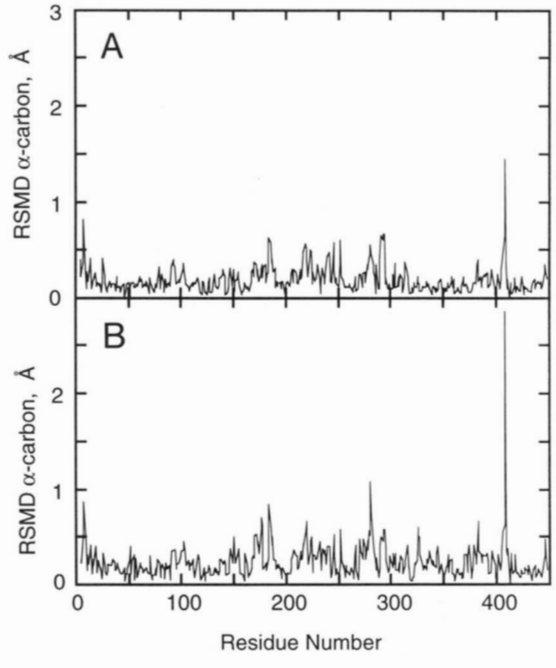

Fig. 2. The RMSD between (**A**) the positions of α-carbon atoms of the H412N(+Zn) and the wild-type structures, and (**B**) the positions of α-carbon atoms of the H412N(−Zn) and the wild-type structures. In each case, the data for the B-chain are shown.

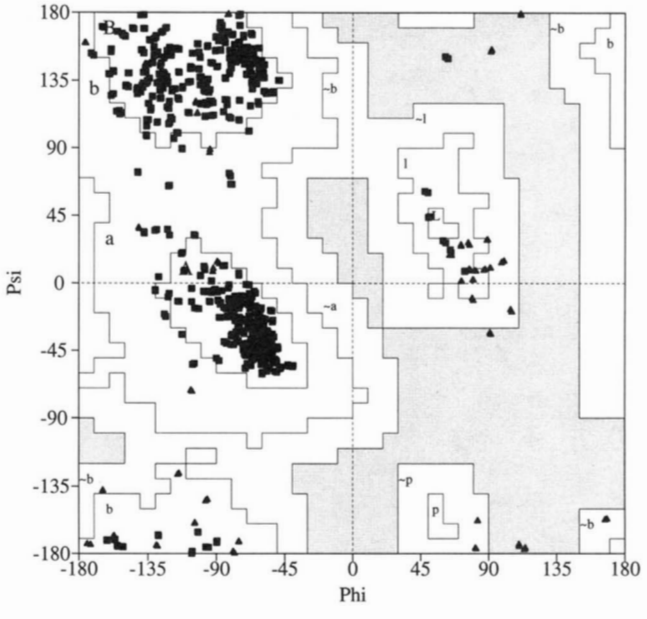

Fig. 4. Ramachandran plot of dihedral angles for the H412N(+Zn) structure. Data show that 90.6% of the 892 residues are in the most favored regions (A, B, L), 9.1% in the additional allowed regions (a, b, l, p), and only 0.3% in the disallowed regions. This figure was prepared using PROCHECK (Laskowski et al., 1993).

slightly in the mutant structure and positioned 2.29 Å away from Zn_2 compared to 2.15 Å away from Zn_2 in the wild-type structure.

Analysis of the area near the Mg site indicated partial and possibly mixed metal occupancy at this site because the electron density maps, as well as the temperature factors and occupancy together, were inconsistent with either full or partially occupied Mg^{2+} at this site. Because of the relatively high concentration of Zn^{2+} in the crystal-stabilizing buffer (10 mM), it is possible that the Mg site was partially occupied by Zn^{2+} and Mg^{2+}.

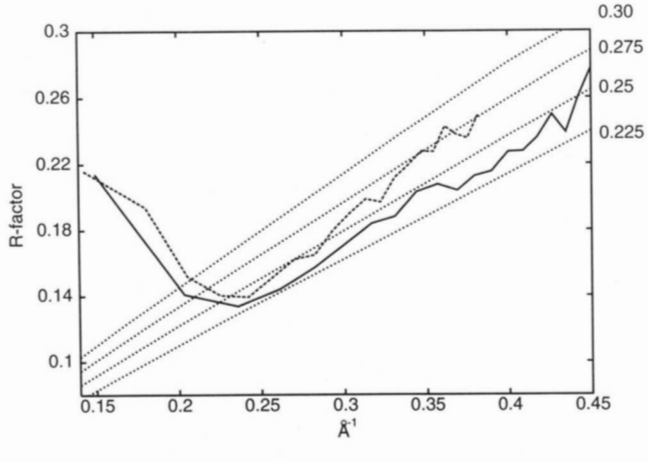

Fig. 3. Luzzati plot showing the final crystallographic *R*-factors, by resolution shell, for H412N(+Zn) (solid line) and H412N(−Zn) (dashed line). The expected uncertainty in the refined X-ray coordinates of both structures is within ±0.22-0.3 Å, as indicated by the set of dashed theoretical lines (Luzzati, 1952).

Structure of H412N alkaline phosphatase at a low concentration of zinc

The structure obtained with the crystals equilibrated at 10^{-7} M Zn^{2+} (H412N[−Zn]) was refined to an *R*-factor of 0.166 at a resolution 2.6 Å. These crystals did not diffract as well as the crystals soaked in stabilizing buffer containing Zn^{2+}. However, the crystals did have the same space group and a similar unit cell size as the wild-type enzyme (Table 2). As was the case for the H412N(+Zn) structure, very weak electron density was observed for the first three residues at the N-terminus of both chains and therefore these residues were not included in the calculations. The Luzzati plot suggested that the error in the coordinates of this structure was approximately ±0.275 Å (see Fig. 3). The H412N(−Zn) structure also had well-refined stereochemistry indicated by the Ramachandran plot (not shown), which was very similar to the one for the H412N(+Zn) structure (Fig. 4).

When the H412N(−Zn) and wild-type structures were compared, there were a significant number of residues that exhibited α-carbon displacements of more than 0.75 Å (Fig. 2B). As seen in Figure 2A, this was not the case for the H412N(+Zn) structure. Analysis of the H412N(−Zn) structure revealed that there were a significant number of differences in the active site region when compared to the structure of the wild-type enzyme (Kim & Wyckoff, 1991); in particular, His-331 and Asn-412 had large displacements.

Closer examination of the Zn_1 site in the H412N(−Zn) structure revealed several structural consequences of the mutation (Fig. 7). The Zn_1 site in the H412N(−Zn) structure appears to be vacant as indicated by a lack of electron density; however, at this resolution, the possibility exists that Zn^{2+} is present at this site at low occupancy. The electron density maps did not indicate a well-defined coordination sphere for Zn_1, support-

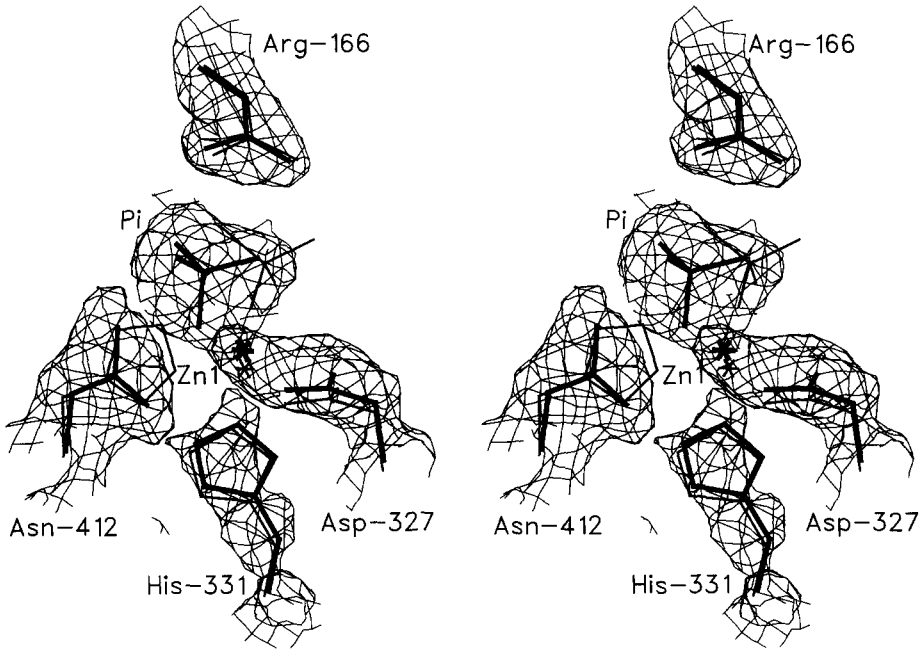

Fig. 5. Stereo view of the $(2F_o - F_c)$ electron density map ($\sigma = 0.8$) at the Zn_1 and phosphate binding sites for the B subunit of the H412N(+Zn) dimer. Refined coordinates of the mutant (thick) and wild-type (thin) structures are superimposed on the electron density maps. This electron density map confirms that the histidine at position 412 has been replaced by asparagine. The Zn_1 site in this structure is approximately 20% occupied. Figures 5–8 were drawn with the program SETOR (Evans, 1993).

ing the conclusion that the Zn_1 was not occupied. Asn-412, the site of the mutation, was in a position similar to that of the imidazole of His-412 in the wild-type enzyme, with the side-chain carbonyl pointing toward the empty Zn_1 site. As was the case for the H412N(+Zn) structure, the position of the phosphate was shifted. The phosphate was held only by the guanidinium group of Arg-166 and the amide nitrogen on the side chain of Asn-412 through hydrogen bonding interactions.

The replacement of His-412 by Asn also influenced the occupancy of the Zn_2 and Mg sites in the H412N(−Zn) structure. The Zn_2 site was only 40% occupied; however, all the ligands to Zn_2 remained in the same relative positions observed in the wild-type structure, with the exception of the phosphate. Although the Mg site in the H412N(−Zn) structure also resembled the Mg site of the wild-type structure, refinement indicated it was only about 80% occupied. Furthermore, there was very weak electron density for Asp-51, which bridges between the Zn_2 and Mg sites, suggesting that this carboxylate side-chain ligand is not well constrained to any particular orientation, which is consistent with the incomplete occupancy of the second and third metal binding sites.

Discussion

His-412 is important for Zn_1 binding and therefore is also important for phosphate and substrate binding

As seen in the H412N(+Zn) and H412N(−Zn) structures (Fig. 8; Kinemage 3), Asn-412 does not project sufficiently into the Zn_1

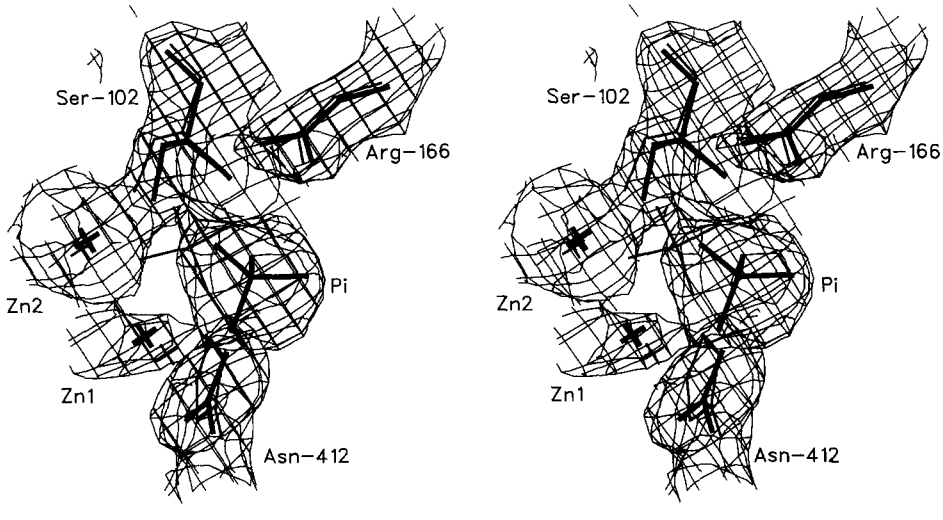

Fig. 6. Stereo view of the $(2F_o - F_c)$ electron density map ($\sigma = 0.8$) at the active site of the H412N(+Zn) enzyme. Refined coordinates of the H412N (thick) and wild-type (thin) structures are superimposed on the electron density maps.

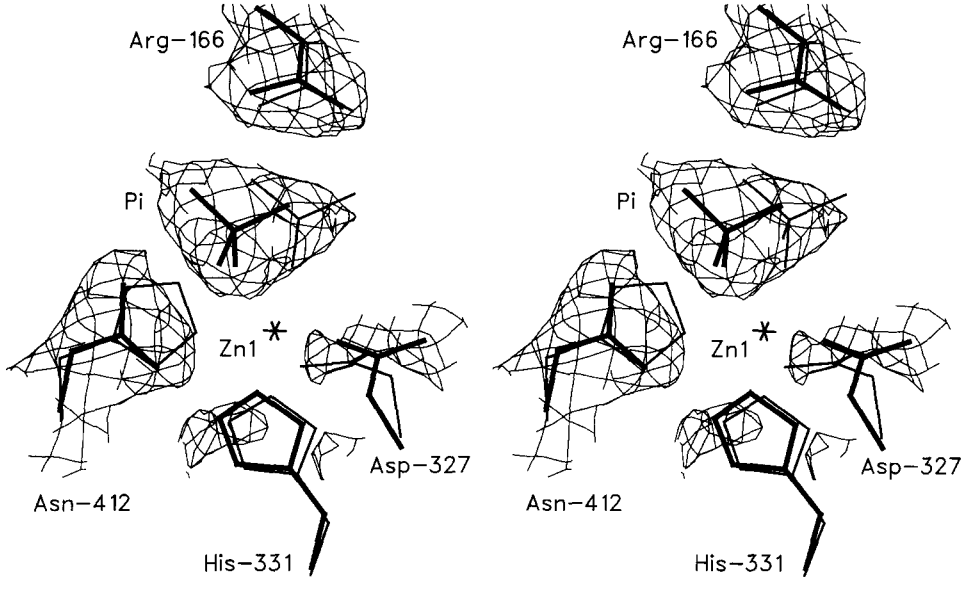

Fig. 7. Stereo view of the $(2F_o - F_c)$ electron density map ($\sigma = 0.6$) at the Zn_1 and phosphate binding sites of the H412N(−Zn) enzyme. Refined coordinates of the H412N (thick) and wild-type (thin) structures are superimposed on the electron density maps. The Zn_1 site is not occupied in the mutant structure, and the density for the ligands His-331 and Asp-327 is very weak.

site to serve as an effective ligand for Zn^{2+}. In this case, asparagine cannot replace histidine as a ligand to zinc; however, it is possible that Gln could successfully replace His because the Gln side chain is longer than the Asn side chain. The lack of an interaction between Asn-412 and Zn_1, observed in these X-ray structures, explains the results from solution studies, which indicated that the H412N enzyme had a reduced affinity for zinc compared to the wild-type enzyme (Ma & Kantrowitz, 1994). From atomic absorption measurements, the residual zinc content of the H412N enzyme was only about 30% of that observed for the wild-type enzyme (Ma & Kantrowitz, 1994). The loss of one interaction between the enzyme and Zn_1 does not destroy the zinc binding site, but it does substantially reduce the affinity of the site for zinc. The weakened binding of Zn_1 is also reflected in increased distances between the zinc and all of its ligands (see Table 4). For example, the distance between the NE2 of His-331 and Zn_1 refined to a value between 0.5 and 1.0 Å longer in the H412N(+Zn) than the wild-type structure, which may represent an average over the liganded and unliganded forms.

The position of Zn_1 also changed due to the absence of the His-412 ligand and the weakened interactions with its other ligands. The alteration in the position of Zn_1 also influenced the position of the phosphate, which moved toward the extra space created by the displacement of Zn_1, allowing it to form a hydrogen bond with the ND2 of Asn-412. In the H412N(+Zn) structure, the phosphate actually has moved away from the substrate binding pocket and become more exposed to the surface

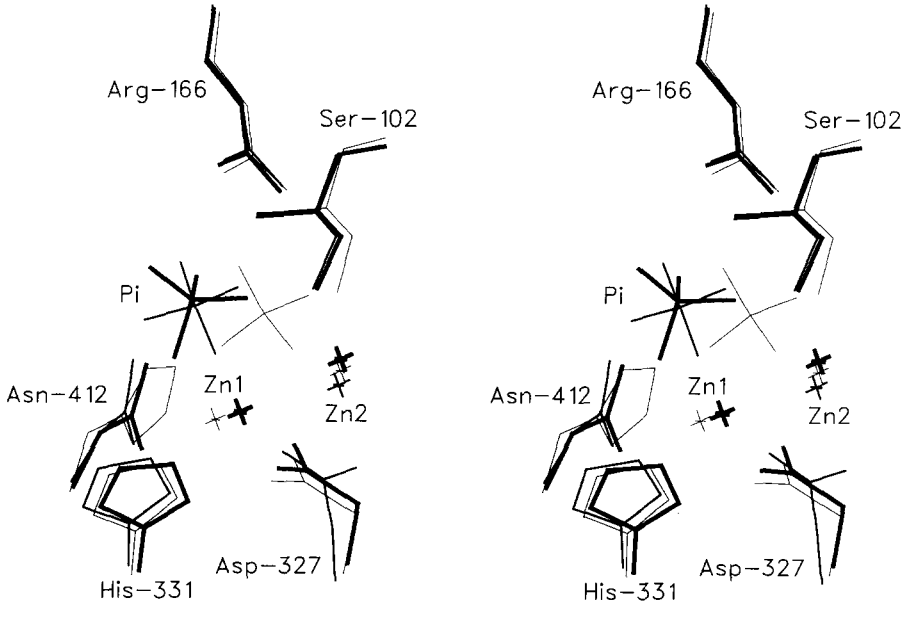

Fig. 8. Comparison of the positions of the active site residues in the H412N(+Zn) (thick line), the H412N(−Zn) (medium line), and the wild-type structures (thin line).

of the protein. The repositioning of the phosphate also resulted in the loss of the interaction between the phosphate and Zn_2 and extended the distance between phosphate and its hydrogen bonding partners (see Table 4).

The weakened interactions between phosphate with its neighbors observed in these two crystal structures explains many of the solution properties of the H412N enzyme, including the observed reduction in phosphate content and affinity, and the increase in phosphate and substrate affinity in the presence of excess zinc.

Comparison of the mutant enzyme structures reveals that the Zn_1 site in the presence of 10 mM Zn^{2+} has a much higher occupancy than the one at low Zn^{2+} (10^{-7} M). As previously reported (Ma & Kantrowitz, 1994), the hydrolysis activity of the H412N enzyme was improved 2.5-fold in k_{cat} and 23-fold in K_m in the presence of 0.2 mM Zn^{2+} compared to the value in the absence of Zn^{2+}. Therefore, the higher activity of the H412N enzyme in the presence of zinc is mainly due to increased zinc binding, which in turn results in increased substrate and phosphate affinity. The ability of zinc to activate the H412N enzyme as well as to enhance substrate binding and phosphate affinity to very close to the wild-type values observed in solution (Ma & Kantrowitz, 1994) correlates well with the structural alterations that occur when zinc is added to the H412N(−Zn) structure.

Replacement of His-412 by Asn disrupts the structural network of the active site

The major differences between the H412N(+Zn) and H412N (−Zn) structures involve the interactions of the protein with the Zn_1 and Zn_2 sites, the interaction of the protein with the phosphate, and the occupancies of the Zn_1 and Zn_2 sites. The positions of the metal atoms in the Zn_2 and Mg sites, as well as the position of the phosphate, were similar in both structures. In the H412N(+Zn) structure, the two zinc atoms refined to somewhat closer together than the 4.0-Å separation observed in the wild-type structure.

Even with optimal amounts of zinc, the k_{cat} of the H412N enzyme is reduced about twofold compared to the value for the wild-type enzyme. This reduction in k_{cat} may be due to the altered position of the phosphate in the mutant structures compared to its position in the wild-type enzyme (see Fig. 8). The phosphate position shifts outward from the binding pocket compared to the wild-type structure. Zn_2 was more than 4.0 Å from the phosphate in both H412N structures and could not interact with the phosphate. In addition, Ser-102 swings slightly toward the phosphate but is still bound to Zn_2. In the wild-type structure, the precise positions of Zn_1, Zn_2, phosphate, and Ser-102 with respect to each other is critical for efficient catalysis. Because the relative positions of Zn_1, Zn_2, phosphate, and Ser-102 in the mutant enzyme have been altered, the precise relationship between these groups required for efficient catalysis has been lost.

Table 4. *Distances between the metals, phosphate, and side-chain ligands in the wild-type and H412N alkaline phosphatases*

		Distance between		Distance (Å)		
				Wild-type	H412N(+Zn)	H412N(−Zn)
Zn_1		His-412	NE2	2.02		
		Asn-412	OD1		3.1[b]	—[a]
		His-331	NE2	2.08	3.2[b]	—[a]
		Asp-327	OD1	2.27	1.8[b]	—[a]
			OD2	2.54	2.7[b]	—[a]
PO_4	O3	Ser-102	OG	2.68	2.99	3.23
	O1	Zn_1		2.04	2.3	
	O2	Zn_2		2.04	—	—
	O3	Arg-166	NH1	2.63	3.26	3.19
	O4	Arg-166	NH2	2.88	3.03	3.13
Zn_2		Asp-51	OD1	2.03	1.89	2.38
		Asp-369	OD1	1.80	1.99	2.23
		His-370	NE2	2.03	1.95	2.28
		Ser-102	OG	2.15	2.29	2.54

[a] Zn_1 was not present in the H412N(−Zn) structure.
[b] The coordinates of the Zn_1 ligands in the H412N(+Zn) structure have a higher uncertainty than would be expected from the Luzzati plot because of the low occupancy of Zn_1.

H412N enzyme has an altered affinity for magnesium

The Mg site of both H412N structures is similar to that observed in the structure of the wild-type enzyme, except that in the H412N(−Zn) structure the Mg site is only partially occupied, and in the H412N(+Zn) structure, there is apparently a mixture of Mg^{2+} and Zn^{2+} bound at this site. For the wild-type enzyme, under the same conditions, the Mg site is fully occupied by Mg^{2+} alone. These data suggest that the affinity of the enzyme for Mg^{2+} has decreased by the replacement of His-412 by Asn. The decreased Mg^{2+} affinity is probably directly related to the disorder observed for Asp-51, which forms a bridge between the Mg and Zn_2 sites. These data also indicate that the three metal binding sites in alkaline phosphatase are closely interrelated on a structural basis. By replacing one of the Zn_1 ligands His-412 by Asn, the Zn_1 binding site is altered, which can then be propagated to the Zn_2 site. Finally, the alteration in the Zn_2 site is transferred to the Mg site via Arg-51, which bridges between these two metal sites. Thus, a small change at one of the metal sites in the enzyme can have profound changes at all of the metal sites. A similar disruption in the coordination of the metals occurred in the enzyme in which Asp-369 was replaced by Asn at the Zn_2 site (Tibbitts et al., 1994).

Binding of Tris weakens zinc binding and reduces the affinity of the enzyme for substrates

The H412N enzyme is inhibited by Tris (Ma & Kantrowitz, 1994) in contrast to the wild-type enzyme, which is activated by Tris due to the additional transferase activity; however, the inhibition of the H412N enzyme by Tris can be reversed by addition of Zn^{2+}. For the wild-type enzyme, Tris acts as a more efficient phosphate acceptor than water, whereas this is not the case for the H412N enzyme. In the structure of the H412N enzyme, the substitution of Asn for His at position 412 actually opens the structure in the region previously occupied by the imidazole of His-412, possibly creating a new Tris binding site. Tris binding in this cavity would prevent Zn from binding to the Zn_1 site,

which in turn would result in a substantial reduction in the affinity of the enzyme for both the phosphorylated substrate and the product phosphate. This loss in substrate affinity is reflected in the increase in K_m observed for this enzyme in the presence of Tris. Based on this model, the effect of Tris on the H412A enzyme, which would be expected to have an even larger pocket near Zn_1 for binding Tris than the H412N enzyme, should be more dramatic. Consistent with this prediction, the H412A enzyme exhibited a 100-fold increase in K_m in the presence of 1 M Tris (Ma & Kantrowitz, 1994).

Summary

The structural studies reported here on the H412N enzyme have been used to understand the solution properties of this mutant enzyme, including its altered substrate affinity, reduced phosphate affinity, low metal content, and low catalytic efficiency. The structural data have also been helpful in suggesting a molecular mechanism for the Tris inhibition of the H412N enzyme, as well as its reversal at high concentrations of Zn^{2+} (Ma & Kantrowitz, 1994). Most of these effects have been caused by creation of a cavity near Zn_1 in the active site pocket. Furthermore, replacement of His-412 with Asn affects all three metal binding sites, perturbing the critical spatial relationship between the positions of the two zinc and Mg^{2+} catalytic cofactors in *E. coli* alkaline phosphatase.

Kinemages

Three kinemages are included: Kinemage 1, to demonstrate the tertiary and quaternary structure of the dimeric *E. coli* alkaline phosphatase as well as the location of the active site; Kinemage 2, to show the coordination of the metals in the active site of the wild-type enzyme; and Kinemage 3, to highlight the differences at the active site between the wild-type and the structures of the H412N alkaline phosphatase, with and without added zinc. The last kinemage permits interactive switching and overlay comparisons of the wild-type, the H412N(−Zn), and H412N(+Zn) X-ray structures.

Materials and methods

Materials

Agar, agarose, ampicillin, *p*-nitrophenyl phosphate, sodium dihydrogen phosphate, magnesium chloride, and zinc chloride were purchased from Sigma Chemical Co. Tris, enzyme-grade ammonium sulfate, and sucrose were supplied by ICN Biomedicals. Tryptone and yeast extract were from Difco Laboratories.

Strains

The Δ*phoA E. coli* K12 strain SM547 (Δ[*phoA-phoC*], *phoR*, tsx::Tn5, Δ*lac*, *galK*, *galU*, *leu*, str^r) was a gift from H. Inouye.

Expression and purification of the H412N alkaline phosphatase

The H412N enzyme was purified as reported previously (Ma & Kantrowitz, 1994) using *E. coli* strain SM547, which had been transformed with plasmid pEK202. *E. coli* SM547 was used as the host strain for expression of the H412N enzyme because this strain contains a chromosomal deletion of the *phoA* gene and a mutation in the *phoR* regulatory gene. Therefore, no contamination from the wild-type alkaline phosphatase was possible.

Crystallization

Crystals were obtained using the hanging drop vapor diffusion method. Before use, the enzyme, at a concentration of approximately 30 mg/mL, was dialyzed against a buffer composed of 20% saturated $(NH_4)_2SO_4$, 100 mM Tris, 10 mM $MgCl_2$, and 0.01 mM $ZnCl_2$ at pH 9.5. Drops of 15 μL were suspended on coverslips and equilibrated with 1 mL of buffer (39% saturating $[NH_4]_2SO_4$, 100 mM Tris, 10 mM $MgCl_2$, pH 9.5). The crystals, which grew in 1–2 weeks, were harvested by transferring them to a stabilization solution containing 65% saturated $(NH_4)_2SO_4$, 100 mM Tris, 10 mM $MgCl_2$, 2 mM NaH_2PO_4, pH 7.5, with or without 10 mM $ZnCl_2$. The crystals were soaked in the stabilizing solution for several days before data collection. Because the drop containing the crystals contained 0.01 mM $ZnCl_2$, zinc concentration in the stabilization solution without added zinc was actually approximately 10^{-7} M.

Data collection and processing

The diffraction data were collected with an Area Detector Systems MARK III system at the Crystallographic Facility in the Chemistry Department of Boston College. The area detector system was controlled by a Micro VAX3500 computer for data collection using a Rigaku RU-200 rotating-anode X-ray generator operated at 50 kV and 150 mA. The instrumental setup has been reported previously (Tibbitts et al., 1994). For the H412N(+Zn) structure, data were collected to 2.2 Å resolution using two crystals. A total of 63,998 unique reflections were obtained from 224,987 measurements, with an average redundancy of 3.5. For the H412N(−Zn) structure, data were collected to 2.6 Å on three crystals that had been soaked in stabilization buffer in the absence of zinc. A total of 177,067 reflections were collected of which 38,252 were unique, giving an average redundancy of 4.6 (Table 2). Diffraction data were merged and processed with the software provided by Area Detector Systems (Hamlin et al., 1981).

Structural refinement

The initial model used to begin the structural refinement was the coordinates of the wild-type *E. coli* alkaline phosphatase (Brookhaven Data Bank file 1ALK), with metals, phosphate, and waters removed. In addition, His-412 was replaced by Asn using QUANTA (Molecular Simulations, Inc., Burlington, Massachusetts). Both crystal structures were refined using X-PLOR (Brünger, 1992; Molecular Simulations, Inc.) running on Silicon Graphics Indigo II workstations at Boston College and on the Cray Y-MP C90 at the Pittsburgh Supercomputer Center. The initial *R*-factors were 0.360 and 0.343 for the H412N(+Zn) and H412N(−Zn) structures, respectively. Subsequent positional refinement and temperature factor refinement improved the *R*-factors and stereochemistry. At this stage, the metals, their water ligands, and phosphate were built in according to the calculated electron density ($2F_o - F_c$) and ($F_o - F_c$) maps using QUANTA. The structures were then further refined by cycles

of positional refinement, temperature factor refinement, and simulated annealing using initial temperatures up to 3,000 °C. An initial set of solvent water molecules was then added from the D369N structure (Protein Data Bank file 1ALH, Tibbitts et al., 1994). During subsequent refinement the temperature factors of the waters were carefully monitored, and water molecules that had temperature factors above 60 Å^2 were deleted. Additional solvent water molecules were added based upon difference Fourier maps ($F_o - F_c$) at several stages, and approximately 230 waters are present in each of the refined structures (Table 3). During refinement, noncrystallographic symmetry constraints (Tibbitts et al., 1994) were also used. Simulated annealing omit maps (Brünger, 1992) were also used to determine the positions of side chains in the active site region of these structures. Coordinates for the H412N(−Zn) and H412N(+Zn) structures have been deposited in the Brookhaven Protein Data Bank as 1ALI and 1ALJ, respectively.

Acknowledgments

This work was supported by grant GM42833 from the National Institute of General Medical Sciences and by Pittsburgh Supercomputing Center grant 1 P41 RR06009 from the NIH National Center for Research Resources. We thank H.W. Wyckoff and E.E. Kim for providing the X-ray coordinates of the wild-type enzyme prior to their deposition in the Brookhaven Protein Data Bank (1ALK). We also thank Dr. B. Stec and Dr. E. Giroux for their helpful discussions.

References

Anderson RA, Bosron WF, Kennedy FS, Vallee BL. 1975. The role of magnesium in *Escherichia coli* alkaline phosphatase. *Proc Natl Acad Sci USA 72*:2989–2993.

Brünger AT. 1992. *X-PLOR, Version 3.1*. New Haven, Connecticut: Yale University Press.

Cathala G, Brunel C, Chappelet-Tordo D, Lazdunski M. 1975. Bovine kidney alkaline phosphatase. Catalytic properties, subunit interactions in the catalytic process, and mechanism of Mg^{2+} stimulation. *J Biol Chem 250*:6046–6053.

Coleman JE. 1992. Structure and mechanism of alkaline phosphatase. *Annu Rev Biophys Biomol Struct 21*:441–483.

Dayan J, Wilson IB. 1964. The phosphorylation of Tris by alkaline phosphatase. *Biochim Biophys Acta 81*:620–623.

Engström L. 1962. Incorporation of inorganic phosphate into alkaline phosphatase from *Escherichia coli*. *Biochim Biophys Acta 56*:606–609.

Evans SV. 1993. SETOR: Hardware-lighted three-dimensional solid representations of macromolecules. *J Mol Graphics 11*:134–138.

Hamlin R, Cork C, Howard A, Nielson C, Vernon W, Mathews D, Xuong N. 1981. Characteristics of a flat multiwire area detector for protein crystallography. *J Appl Crystallogr 14*:85–93.

Janeway CML, Xu X, Murphy JE, Chaidaroglou A, Kantrowitz ER. 1993. Magnesium in the active site of *Escherichia coli* alkaline phosphatase is important for both structural stabilization and catalysis. *Biochemistry 32*:1601–1609.

Kim EE, Wyckoff HW. 1991. Reaction mechanism of alkaline phosphatase based on crystal structures. *J Mol Biol 218*:449–464.

Laskowski RA, MacArthur MW, Moss DS, Thornton JM. 1993. PROCHECK: A program to check the stereochemical quality of protein structures. *J Appl Crystallogr 26*:283–291.

Luzzati PV. 1952. Traitement statistique des erreurs dans la determination des structures cristallines. *Acta Crystallogr 5*:802–810.

Ma L, Kantrowitz ER. 1994. Mutations at histidine 412 alter zinc binding and eliminate transferase activity in *Escherichia coli* alkaline phosphatase. *J Biol Chem 269*:31614–31619.

Murphy JE, Xu X, Kantrowitz ER. 1993. Conversion of a magnesium binding site by a single amino acid substitution in *Escherichia coli* alkaline phosphatase. *J Biol Chem 268*:21497–21500.

Schwartz JH, Lipmann F. 1961. Phosphate incorporation into alkaline phosphatase of *E. coli*. *Proc Natl Acad Sci USA 47*:1996–2005.

Simpson RT, Vallee BL. 1968. Two differentiable classes of metal atoms in alkaline phosphatase of *E. coli*. *Biochemistry 7*:4343–4349.

Sowadski JM, Handschumacher MD, Murthy HMK, Foster BA, Wyckoff HW. 1985. Refined structure of alkaline phosphatase from *Escherichia coli* at 2.8 Å resolution. *J Mol Biol 186*:417–433.

Sowadski JM, Handschumacher MD, Murthy HMK, Kundrot C, Wyckoff HW. 1983. Crystallographic observations of the metal ion triple in the active site of alkaline phosphatase. *J Mol Biol 170*:575–581.

Tibbitts TT, Xu X, Kantrowitz ER. 1994. Kinetics and crystal structure of a mutant *Escherichia coli* alkaline phosphatase (Asp-369 → Asn): A mechanism involving one zinc per active site. *Protein Sci 3*:2005–2014.

Wilson IB, Dayan J, Cyr K. 1964. Some properties of alkaline phosphatase from *Escherichia coli*. Transphosphorylation. *J Biol Chem 239*:4182–4185.